Traffic 2006; 7: 1060–1077
Blackwell Munksgaard

doi: 10.1111/j.1600-0854.2006.00442.x

Vesicular Trafficking of Semaphorin 3A is Activity-Dependent and Differs Between Axons and Dendrites

Joris de Wit[1], Ruud F. Toonen[1], Joost Verhaagen[2] and Matthijs Verhage[1,*]

[1]Department of Functional Genomics, Center for Neurogenomics and Cognitive Research (CNCR), Vrije Universiteit (VU) and VU Medical Center (VUmc), De Boelelaan 1087, 1081 HV Amsterdam, the Netherlands
[2]Neuroregeneration Laboratory, Netherlands Institute for Brain Research, Meibergdreef 33, 1105 AZ Amsterdam, Amsterdam, the Netherlands
**Corresponding author: Matthijs Verhage, matthijs@cncr.vu.nl*

Secreted semaphorins act as guidance cues in the developing nervous system and may have additional functions in mature neurons. How semaphorins are transported and secreted by neurons is poorly understood. We find that endogenous semaphorin 3A (Sema3A) displays a punctate distribution in axons and dendrites of cultured cortical neurons. GFP–Sema3A shows a similar distribution and co-localizes with secretory vesicle cargo proteins. Live-cell imaging reveals highly dynamic trafficking of GFP–Sema3A vesicles with distinct properties in axons and dendrites regarding directionality, velocity, mobility and pausing time. In axons, most GFP–Sema3A vesicles move fast without interruption, almost exclusively in the anterograde direction, while in dendrites many GFP–Sema3A vesicles are stationary and move equally frequent in both directions. Disruption of microtubules, but not of actin filaments, significantly impairs GFP–Sema3A transport. Interestingly, depolarization induces a reversible arrest of axonal transport of GFP–Sema3A vesicles but has little effect on dendritic transport. Conversely, action potential blockade using tetrodotoxin (TTX) accelerates axonal transport, but not dendritic transport. These data indicate that axons and dendrites regulate trafficking of Sema3A and probably other secretory vesicles in distinct ways, with axons specializing in fast, uninterrupted, anterograde transport. Furthermore, neuronal activity regulates secretory vesicle trafficking in axons by a depolarization-evoked trafficking arrest.

Key words: axon guidance, axonal transport, large dense core vesicle, live-cell imaging, plasticity, secretory granule, semaphorin

Received 22 September 2005, revised and accepted for publication 19 April 2006, published on-line 25 May 2006

Secreted semaphorins are essential for the proper wiring of the developing nervous system (1). Semaphorin 3A (Sema3A) is a secreted guidance molecule that acts as a chemorepellent for axonal growth cones (2). The effects of secreted semaphorins in the nervous system are mediated by a receptor complex consisting of ligand-binding neuropilin-1 (Npn-1) or Npn-2 and signal-transducing plexins (3). Activation of the receptor complex initiates an intricate signaling cascade leading to reorganization of the cytoskeleton (4). *Sema3A* and *Sema3F* null mutant mice show extensive defasciculation of peripheral projections and guidance defects in the central nervous system (CNS) (5–7), which are largely phenocopied in null mutants of their respective receptor components Npn-1 and Npn-2 (8–10). Both Sema3A and Sema3F continue to play a role in the wiring of the postnatal brain by promoting pruning of specific hippocampal projections (11).

Recent evidence indicates that the role of secreted semaphorins may extend beyond defining the connectivity pattern of the developing brain (12). Sema3A stimulates growth and branching of cortical dendrites in slice cultures (13), and secreted semaphorin-Npn-1 signaling has been shown to regulate the complexity of cortical basal dendrites *in vivo* (14). Expression of secreted semaphorins persists in adult neurons (15,16) and can be modulated by electrical activity (17,18). Moreover, the secreted semaphorin Sema3F can alter synaptic transmission in adult hippocampal slices (19). Together, these studies suggest a role for secreted semaphorins in structural and synaptic plasticity. However, how secreted semaphorins exert their effects on dendritic complexity and synaptic transmission is unclear, as it is unknown how semaphorins are transported and released by neurons. Furthermore, whether transport of secreted semaphorins depends on neuronal activity is unresolved.

Here, we investigated the trafficking of the secreted semaphorin Sema3A in cortical neurons. *Sema3A* is highly expressed in the developing neocortex (20,21) and continues to be expressed in subpopulations of cortical neurons in adulthood (15). We show that a previously characterized GFP–Sema3A fusion protein (22) closely reproduces the punctate distribution of the endogenous protein in cortical neurons and is transported in secretory vesicles along microtubules. Live-cell imaging of transfected neurons revealed striking differences in the dynamics of GFP–Sema3A vesicular trafficking in axons and dendrites. Compared to axonal vesicles, dendritic GFP–Sema3A vesicles moved slower, paused more frequently and were often stationary. Furthermore, axonal trafficking of GFP–Sema3A was strongly influenced by neuronal activity, whereas dendritic trafficking was not. Thus, both the dynamics and the activity dependence of GFP–Sema3A trafficking in neurons differ between axons

and dendrites. These data indicate that axons and dendrites regulate trafficking of Sema3A and probably other secretory vesicles in distinct ways.

Results

Punctate distribution of endogenous Sema3A in axons and dendrites of cortical neurons

We first analyzed the localization of endogenous Sema3A protein in neurons. Cultured neurons derived from E18 entorhinal and piriform cortex, cortical regions with high Sema3A expression during embryonic development (20,21), were used. The Sema3A C-17 antibody (Ab) used is directed against epitopes in the C-terminus of Sema3A. At 6 days *in vitro* (DIV), prominent Sema3A labeling was observed in axons and growth cones (Figure 1A). Sema3A puncta displayed a similar distribution as synapsin-positive synaptic vesicles (Figure 1B), which were present in the axon shaft and accumulated in the growth cones of immature neurons (23). Despite their similar distribution, Sema3A puncta showed little colocalization with synaptic vesicles in growth cones and neurites (Figure 1C), suggesting that Sema3A is sorted to a distinct vesicular compartment. In more mature neurons (17 DIV), Sema3A showed a punctate distribution in cell body and neurites (Figure 1D). Microtubule-associated protein-2 (MAP2) labeling was used to identify the somatodendritic compartment (Figure 1E). Discrete Sema3A-positive puncta localized to both MAP2-positive dendrites and MAP2-negative axons (Figure 1F,H). A similar punctate distribution in neurons was found using two different Abs against Sema3A (data not shown). In addition to the labeling in neurites, a punctate Sema3A labeling outlined the membrane of neuronal cell bodies (Figure 1G), suggesting association with the cell surface in this compartment. To confirm the specificity of the Ab used, we stained neurons expressing recombinant GFP–Sema3A (22) with the Sema3A C-17 Ab. Extensive overlap between Sema3A Ab staining and GFP–Sema3A

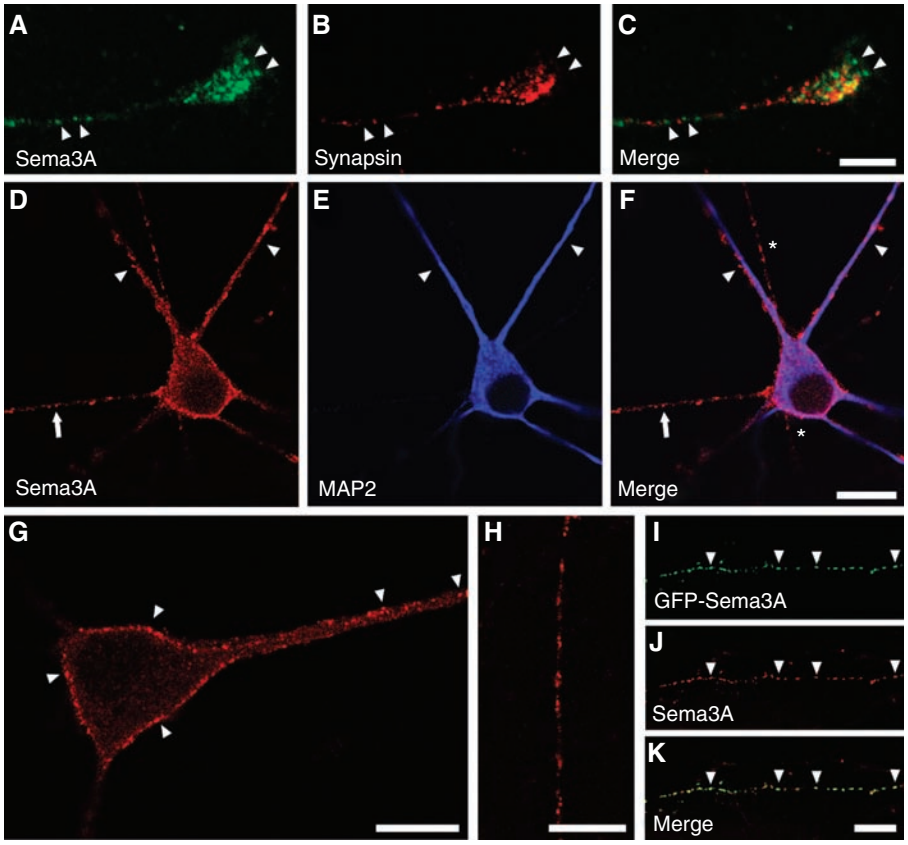

Figure 1: Endogenous Sema3A shows a punctate distribution in neurites of cortical neurons. A–C, axonal growth cone (6 DIV) labeled with Sema3A C-17 (A) and synapsin (B) antibodies. A, Sema3A-positive puncta in axon and growth cone (arrowheads). B, Synapsin labeling. C, Merged image. D, Sema3A immunocytochemistry on mature neuron (17 DIV). E, MAP2 staining identifies dendrites (arrowheads). F, Merged image shows punctate Sema3A distribution in both dendrites and axons (arrow). Asterisks indicate another axon extending along neuron in (F). G, Sema3A-positive puncta outline the cell body and are present in dendrite (arrowheads). MAP2 signal not shown. H, Detail of axon-showing punctate Sema3A labeling. I, GFP–Sema3A expressed in cortical neuron (10 DIV). Image shows segment of axon. J, Sema3A immunocytochemistry of the axon shown in (I). K, Merged image shows extensive overlap of GFP–Sema3A fluorescence and Sema3A antibody staining in yellow (indicated with arrowheads). Scale bar in (A–C) is 5 μm and in (D–K) is 10 μm.

fluorescence was observed, showing that the Ab recognizes Sema3A (Figure 1I–K).

GFP–Sema3A mimics the punctate distribution of Sema3A in cortical axons and dendrites

Expression of GFP–Sema3A in cortical neurons resulted in a characteristic punctate distribution of GFP–Sema3A fluorescence, similar to endogenous Sema3A (Figure 2). Discrete GFP–Sema3A puncta localized to axons and growth cones of DIV 6 neurons (Figure 2A) and showed little co-localization with synaptic vesicles (Figure 2C), consistent with the distribution of endogenous Sema3A (Figure 1A–C). A punctate GFP–Sema3A distribution was also observed in cell bodies and dendrites of DIV 6 neurons (Figure 2D–G). In more mature neurons (DIV 14), GFP–Sema3A puncta were observed in both axons and dendrites and could be detected at large distances from the cell body (Figure 2H–O). GFP–Sema3A puncta were occasionally found in the vicinity of presynaptic terminals (Figure 2L–O). Quantification showed that 18.9 $\pm$ 3.2% (mean $\pm$ SEM) of synapsin-labeled terminals partially overlapped with GFP–Sema3A puncta ($n = 586$ synapses measured in three cells). Thus, the expression of GFP–Sema3A in cortical neurons results in a punctate distribution that closely mimics that of the endogenous protein.

Sema3A is transported in secretory vesicles

Because Sema3A is a secreted protein, we co-expressed fluorescent versions of Sema3A with fluorescently labeled vesicle cargo proteins to determine whether the Sema3A puncta in neurons represent a vesicular compartment. Monomeric red fluorescent protein (mRFP)–Sema3A showed a punctate distribution in neurons (Figure 3A), identical to that of GFP–Sema3A (data not shown). mRFP–Sema3A was co-expressed with tissue plasminogen activator–GFP (tPA–GFP), which is transported in secretory vesicles of the regulated secretory pathway in neuroendocrine cells and hippocampal neurons (24,25). In

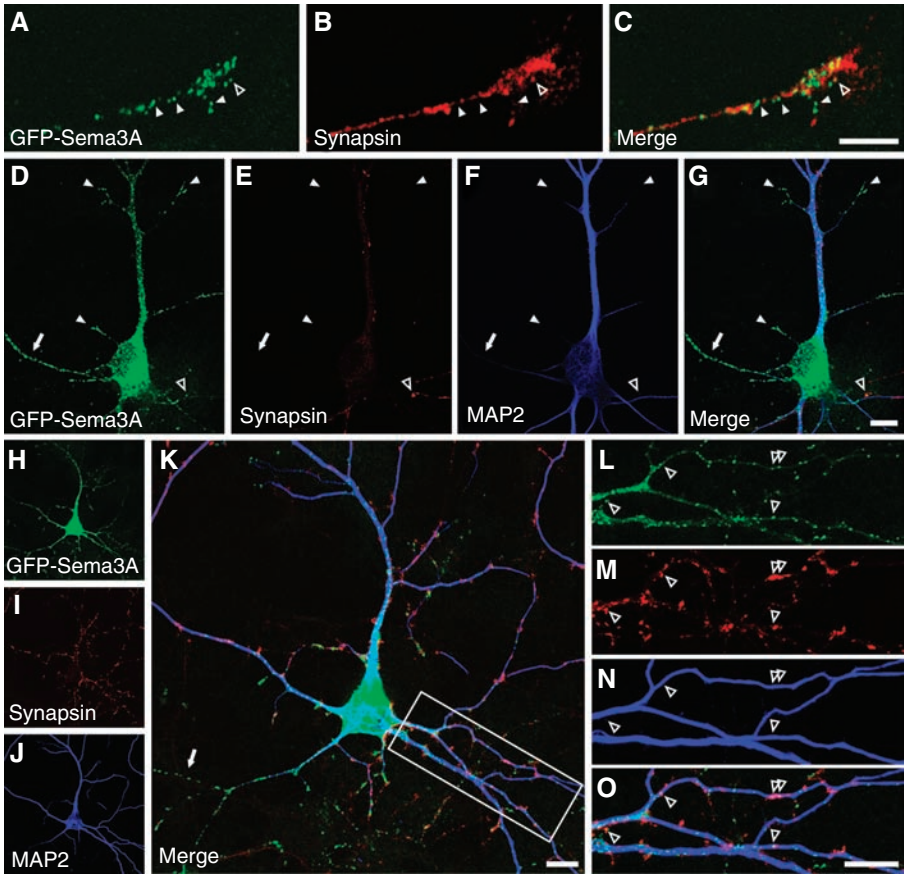

Figure 2: Punctate localization of GFP–Sema3A in neurites of cortical neurons. A–C, Axonal growth cone (6 DIV). A, GFP–Sema3A puncta (arrowheads) in axon and growth cone. B, Synapsin labeling. C, Merged image. Open arrowhead indicates co-localization. D–G, Cortical neuron (6 DIV), transfected at DIV 3. D, GFP–Sema3A. GFP–Sema3A puncta are present in axon (indicated with arrow), dendrites and dendritic growth cones (arrowheads). E, Synapsin labeling. F, MAP2 labeling. G, Merged image. GFP–Sema3A puncta occasionally co-localize with synapses (open arrowhead). H–O, Cortical neuron (DIV 14). H, GFP–Sema3A. I, Synapsin labeling. J, MAP2 labeling. K, Merged image. Arrow indicates axon. L–O, Higher magnification of boxed image in (K). L, GFP–Sema3A. M, Synapsin labeling. N, MAP2 labeling. O, Merged image. Some dendritic GFP–Sema3A puncta are localized in the vicinity of synapses (open arrowheads). Scale bar in (A–C) is 5 μm and in (D–O) is 10 μm.

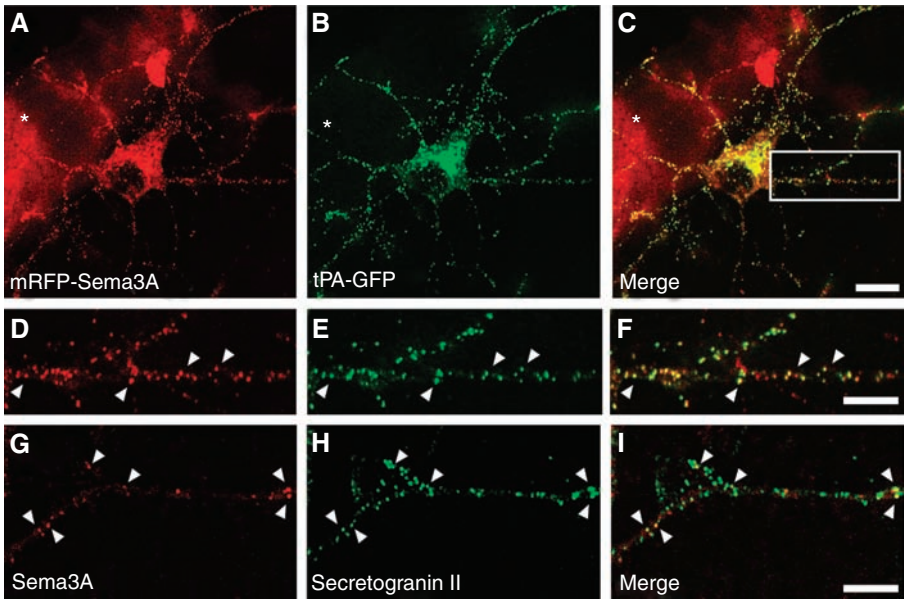

Figure 3: Sema3A is transported in secretory vesicles. A–F, Cortical neuron (DIV 6) co-transfected with mRFP–Sema3A (A,D) and secretory granule marker tPA–GFP (B,E) at DIV 3. Note the characteristic labeling of the extracellular substrate by mRFP–Sema3A (indicated with asterisk), but not by tPA–GFP. Merged image (C,F) shows extensive co-localization (yellow). D–F, Higher magnification of boxed area in (C). Arrowheads indicate co-localizing puncta of mRFP–Sema3A and tPA–GFP. G–I, DIV 6 cortical neuron double-labeled with Sema3A antibody (G) and SgII antibody (H). Merged image (I) shows co-localization of Sema3A and SgII-positive puncta (indicated with arrowheads). Scale bar in (A–C) is 20 μm and in (D–I) is 5 μm.

cortical neurons, tPA–GFP displayed a punctate distribution in cell bodies and neurites (Figure 3B). We observed an extensive co-localization of mRFP–Sema3A with tPA–GFP (Figure 3A–F). Quantification showed that 88.1 ± 5.7% of mRFP–Sema3A puncta overlapped with tPA–GFP ($n = 222$ puncta in five cells). Similar co-localization values were obtained for both axons and dendrites. Co-expression of mRFP–Sema3A with neuropeptide Y–Venus, another secretory vesicle cargo protein (25–27), also resulted in extensive co-localization (88.8 ± 4.2% overlap; $n = 230$ puncta in five cells). In contrast, GFP–Sema3A showed a modest co-localization with the presynaptic marker VAMP–mRFP in axons (22.0 ± 7.6% overlap; $n = 154$ puncta in four cells), and little co-localization was observed between GFP–Sema3A and transferrin-labeled endosomes in dendrites (11.0 ± 1.7% overlap; $n = 246$ puncta in four cells). Thus, mRFP–Sema3A is transported in the same type of vesicle as the exogenously expressed secretory vesicle cargo proteins tPA–GFP and NPY–Venus. To analyze whether endogenous Sema3A localizes to secretory vesicles in neurons, we performed double immunocytochemistry for Sema3A and secretogranin II (SgII), a secretory granule marker. This revealed a partial co-localization in cortical neurons (Figure 3G–I). Quantification showed that 42.3 ± 3.2% ($n = 213$ puncta in five cells) of Sema3A-positive puncta co-localized with SgII-labeled puncta. Similar values were obtained for both axons and dendrites. We attempted to confirm the localization of endogenous Sema3A to secretory vesicles at the ultrastructural level, but localization studies at the electron microscopic level using immunogold proved not feasible with the currently available Ab (data not shown).

Sema3A was originally isolated from brain membrane fractions (2). To determine whether some GFP–Sema3A puncta may reside on the neuronal cell surface, we labeled living, non-permeabilized neurons with an anti-GFP Ab. Live labeling revealed bright clusters of GFP fluorescence on the surface of dendrites of GFP–Sema3A-expressing neurons (Figure 4A–D). Surface expression of GFP–Sema3A was also observed on axons (Figure 4E), as well as on cell bodies (Figure 4F–H), where the punctate staining outlining the cell body was reminiscent of the distribution of endogenously expressed Sema3A (Figure 1G). Attempts to label endogenous Sema3A on the cell surface with three different Abs were unsuccessful (data not shown). The punctate cell surface distribution of GFP–Sema3A was specific, because surface labeling was absent on neurons expressing GFP alone (Figure 4I–K). The surface expression of GFP–Sema3A suggests that GFP–Sema3A can be secreted from both axons and dendrites and subsequently bind to negative charges on the cell surface (22). To test whether secreted GFP–Sema3A might be released and subsequently endocytosed by neighboring non-transfected neurons, cultured neurons were incubated with GFP–Sema3A-conditioned medium (CM), obtained from GFP–Sema3A-expressing HEK293 cells (22). GFP–Sema3A CM did not produce a detectable punctate staining in neurons and did not co-localize with

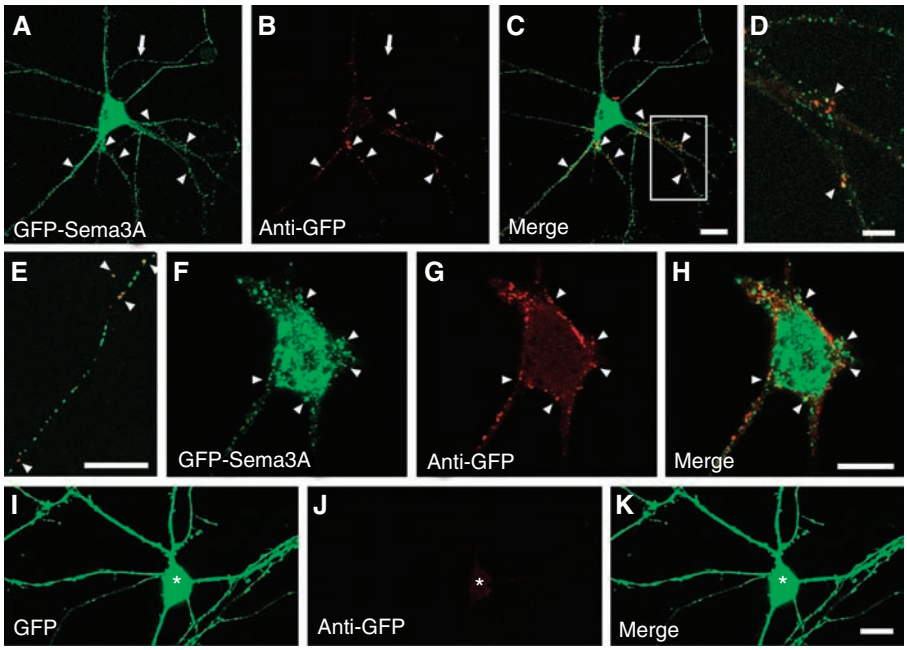

Figure 4: Sema3A puncta localize to the neuronal cell surface and cytoplasm. A–D, Cortical neuron (16 DIV) live-labeled with an anti-GFP antibody. A, GFP–Sema3A. B, Anti-GFP labeling. C, Merged image shows dendritic surface GFP–Sema3A clusters in yellow (indicated with arrowheads). Arrow indicates axon. D, Higher magnification of boxed area in (C) showing surface GFP–Sema3A clusters on dendrite (arrowheads). E, Detail of axon showing GFP–Sema3A surface clusters in yellow (arrowheads). F–H, Surface GFP–Sema3A clusters outlining the cell body (arrowheads). Some clusters appear red but not green due to the sensitivity of anti-GFP staining that yields a stronger signal than that of GFP–Sema3A fluorescence. I–K, GFP–Sema3A surface staining is specific because live-cell labeling of GFP-expressing neurons with GFP antibody shows no surface expression. Asterisk in (I–K) indicates the position of the cell body. Scale bar in (A–C; E–K) is 10 μm and in (D) is 5 μm.

simultaneously added transferrin (data not shown). The only labeling observed was on the surface of glial cells on which the neurons were grown, similar to the fluorescent halo often observed around XFP–Sema3A-expressing neurons (Figure 3A). This suggests that secreted GFP–Sema3A adheres mainly to the surface and substrate of the transfected neuron and does not produce a punctate distribution in neighboring non-transfected cells.

Live-cell imaging reveals distinct characteristics of GFP–Sema3A trafficking in axons and dendrites

To analyze the dynamics of GFP–Sema3A vesicle transport in cortical neurons, we imaged live GFP–Sema3A-expressing neurons. Figure 5A shows frames of a time-lapse movie of GFP–Sema3A trafficking in an axonal segment (*Supplementary* Movie 1). The identity of axons and dendrites of imaged neurons was confirmed by retrospective labeling for MAP2 (data not shown). Vesicles displayed rapid movements in both the anterograde and the retrograde direction, sometimes interrupted by stationary periods, and could be observed to merge, separate or suddenly change direction. GFP–Sema3A carriers were invariably spherical in shape. The positions of three representative vesicles are indicated in Figure 5A to illustrate different types of movement. Some axonal vesicles remained stationary during imaging (vesicle 1), but most moved in the anterograde direction (vesicle 2). In addition, some vesicles changed their direction several times during imaging (vesicle 3) or moved in the retrograde direction. The corresponding kymograph of this axonal segment is shown in Figure 5C, and the trajectories of the numbered vesicles indicated in Figure 5A have been highlighted. The majority of axonal GFP–Sema3A vesicles displayed continuous movement in the anterograde direction, with few stationary puncta (Figure 5C). Dendritic transport of GFP–Sema3A was far less dynamic (Figure 5B, *Supplementary* Movie 2). Most vesicles in this time-lapse sequence remained stationary during the course of imaging (vesicle 1). The vesicles that did move often displayed only small movements (vesicle 3) or changed their direction several times (vesicle 2). The corresponding kymograph shows that vertical lines of stationary vesicles are dominant in dendrites and that continuous movements in the anterograde direction are largely absent (Figure 5D). The difference in dynamics of GFP–Sema3A trafficking in axons and dendrites is readily observed when both kymographs are compared (Figure 5C,D).

To quantify the dynamics of GFP–Sema3A trafficking, individual GFP–Sema3A vesicles in axons and dendrites were manually tracked. We discerned four categories of movement: anterograde and retrograde vesicles, bi-directional (vesicles that changed direction during the course of imaging) and stationary vesicles. Velocities were corrected for stationary periods and defined as the total distance

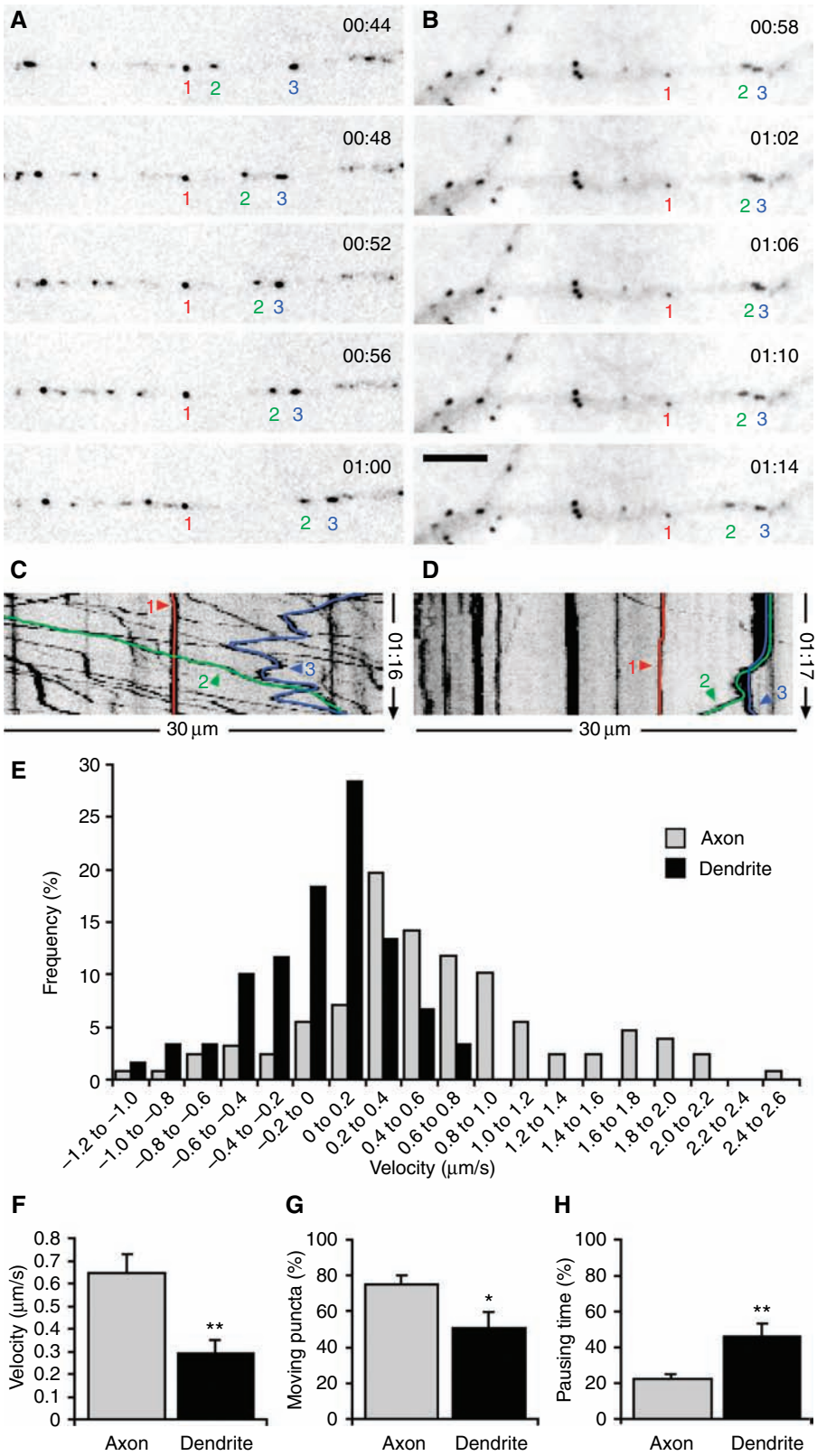

Figure 5: Legend continued on next page

Table 1: Velocities and contribution to total transport of GFP–Sema3A vesicles in axons and dendrites

	Velocity (μm/s)	% of total
Axon		
Anterograde	0.78 ± 0.10	52.7
Retrograde	0.43 ± 0.11	9.3
Bi-directional	0.23 ± 0.02	13.1
Stationary	–	24.9
Dendrite		
Anterograde	0.23 ± 0.05	13.8
Retrograde	0.34 ± 0.08	12.9
Bi-directional	0.26 ± 0.04	26.2
Stationary	–	47.1

Data based on $n = 6$ cells, 430 vesicles tracked. Values represent mean ± SEM.

traveled divided by the time spent moving. A frequency histogram plotting the velocities of GFP–Sema3A vesicles moving in the anterograde and retrograde direction shows that the velocity distributions for axonal and dendritic vesicles were distinct [Figure 5E; $p < 0.001$, Kolmogorov–Smirnov (KS) test]. Anterograde transport in axons was faster than in dendrites, and a population of fast anterograde moving axonal vesicles reached maximum velocities of 2.6 μm/s (Figure 5E). The average velocity of anterograde vesicles was 0.78 ± 0.10 μm/s (mean ± SEM) in axons compared with 0.23 ± 0.05 μm/s in dendrites (Table 1). The value of 0.78 μm/s is consistent with previously reported velocities for anterograde axonal transport vesicles carrying membrane proteins in sensory neurons (28). Similar values were obtained for vesicles carrying NPY–Venus (data not shown). The majority of axonal vesicles moved in the anterograde direction (Table 1), resulting in net anterograde transport of GFP–Sema3A vesicles in axons. Because trafficking in the initial dendritic segment was often too dense to distinguish individual vesicles, we measured the trafficking of vesicles in proximal dendrites at least 20 μm away from the cell body. In contrast to axonal vesicles, dendritic vesicles did not display a clear preference for the anterograde or retrograde direction and a large percentage moved bi-directionally (Table 1).

A comparison of GFP–Sema3A transport characteristics in axons and dendrites showed significant differences for all three parameters examined. First, the average velocity of all moving vesicles was significantly higher in axons than in dendrites (0.65 ± 0.08 μm/s in axons versus 0.29 ± 0.05 μm/s in dendrites; $p = 0.003$; Figure 5F). Second, axons contained more mobile vesicles than dendrites (74.9 ± 4.8% moving vesicles in axons versus 50.9 ± 7.8% in dendrites; $p = 0.025$; Figure 5G). Third, moving vesicles in dendrites had longer pausing times (defined as the time vesicles were stationary divided by the total time a moving vesicle could be followed) than axonal vesicles (22.2 ± 1.5% paused time in axons versus 46.0 ± 6.6% in dendrites; $p = 0.005$; Figure 5H). Thus, dendritic GFP–Sema3A-containing vesicles move slower, are less mobile and pause more frequently than axonal vesicles.

Microtubule-dependent axonal transport of GFP–Sema3A

To determine whether Sema3A vesicular transport depends on an intact cytoskeleton, GFP–Sema3A-expressing neurons were treated for 1 h with cytoskeleton-disrupting drugs and subsequently imaged in the presence of the drug. The microtubule network (visualized with an anti-tubulin Ab) and actin cytoskeleton (visualized with phalloidin) of a representative vehicle-treated neuron are shown in Figure 6A and D, respectively. Treatment with the microtubule-depolymerizing agent nocodazole (10 μM) reduced the tubulin labeling in axons and dendrites (Figure 6B) but did not affect the actin cytoskeleton in the same neuron (Figure 6E). Nocodazole treatment did not completely disrupt the microtubule network. Higher doses of nocodazole (33 μM) were more effective but also severely disturbed neuronal morphology (data not shown). In addition, a higher dose of nocodazole has

Figure 5: Distinct characteristics of GFP–Sema3A trafficking in axons versus dendrites. A,B, Frames from time-lapse movies showing axonal (A) and dendritic (B) trafficking of GFP–Sema3A in cortical neurons (DIV 14–17). Cell bodies are located to the left outside of the picture frame. Images have been inverted for clarity. A, Numbers indicate the positions of a stationary vesicle (1, red), an anterograde vesicle (2, green) and a vesicle moving back and forth (3, blue). B, Numbers indicate the positions of a stationary vesicle (1, red), a vesicle moving back and forth (2, green) and a vesicle displaying a short retrograde displacement (3, blue). The identity of axons and dendrites was verified by retrospective immunocytochemistry for MAP2 (data not shown). C, Kymograph plotting GFP–Sema3A fluorescence on a line drawn along the axonal segment shown in (A) for each movie frame. The trajectories of the numbered vesicles indicated in (A) are highlighted in the corresponding colors. Stationary vesicles appear as vertical lines, and anterograde vesicles appear as downward sloping lines. Most vesicles display continuous anterograde movement. D, Kymograph depicting GFP–Sema3A transport in the dendritic segment is shown in (B). The trajectories of the numbered vesicles indicated in (B) are highlighted in the corresponding colors. Most vesicles are stationary, and uninterrupted movement is largely absent. E, Frequency histogram showing velocities of anterograde and retrograde (indicated as negative values) moving vesicles in axons (grey bars) versus dendrites (black bars). Velocities are defined as the total distance traveled divided by the time spent moving. F, The average velocity of all moving vesicles (anterograde, retrograde and bi-directional) is significantly lower in dendrites compared with axons. G, The percentage moving puncta is significantly lower in dendrites compared with axons. H, The pausing time of moving vesicles (expressed as the time vesicles were stationary divided by the total time a moving vesicle could be followed) is significantly higher in dendrites than in axons. All vesicles visible in the first frame of time-lapse movies were manually tracked through the entire movie or as long as they could be followed. $N = 6$ cells, 430 vesicles tracked. Bar graphs show mean ± SEM. *$p < 0.05$; **$p < 0.01$, Student's *t*-test. Scale bar in (A,B) is 5 μm.

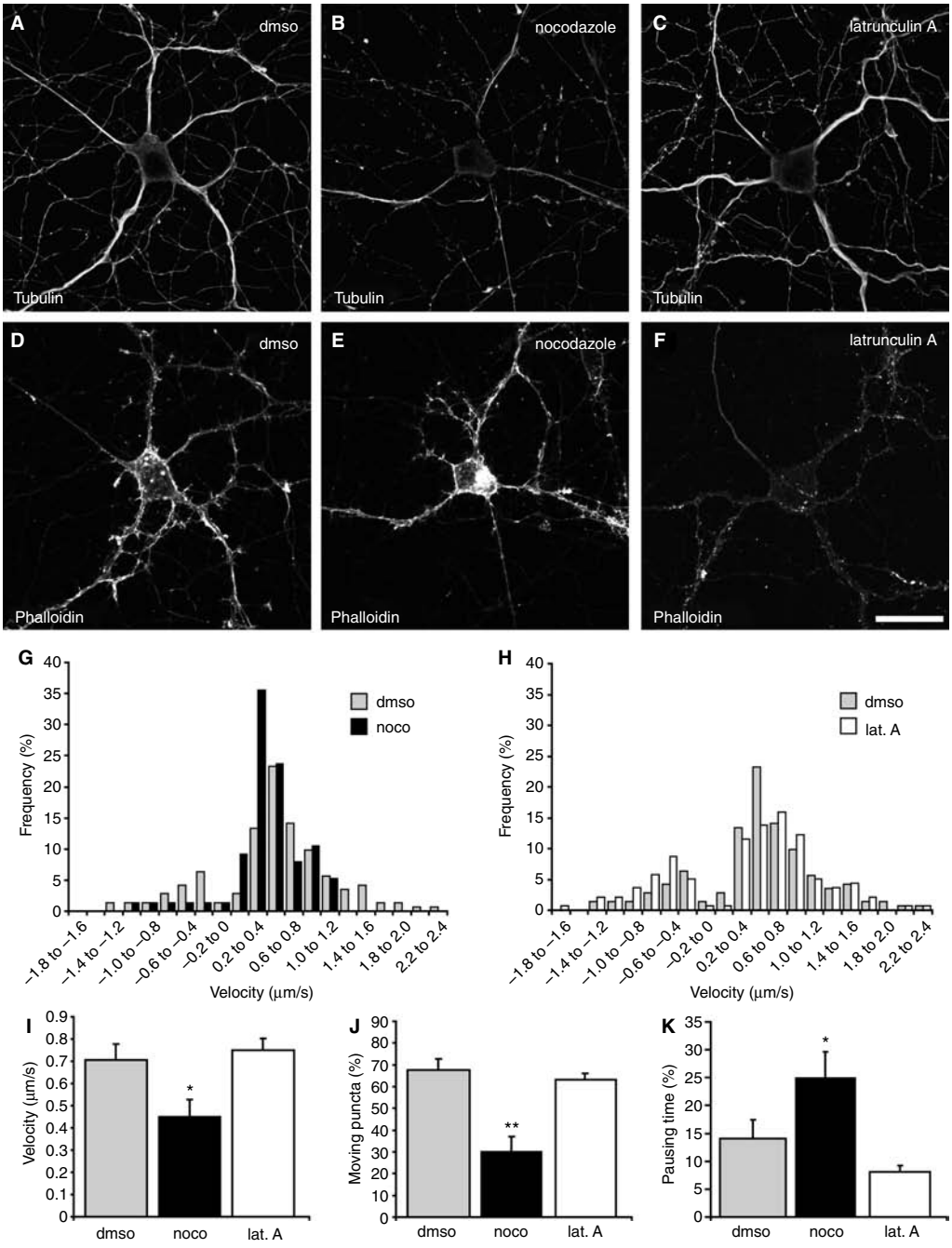

Figure 6: Microtubule-based transport of GFP–Sema3A in cortical neurons. Neurons (DIV 15–16) were treated for 1 h at 37 °C with vehicle (dmso), 10 μM nocodazole (noco) or 5 μM latrunculin A (lat. A) and subsequently imaged in the presence of the drug. A–C, Anti-tubulin-stained microtubule networks of a vehicle-treated neuron (A), nocodazole-treated neuron (B) and latrunculin A-treated neuron (C). D–F, Phalloidin-labeled actin cytoskeleton of the same neurons shown in (A–C). Images of different treatment conditions were taken with identical settings. G, Frequency histogram showing velocities of anterograde and retrograde (indicated as negative values) moving vesicles in axons of vehicle- (grey bars) and nocodazole- (black bars) treated neurons. H, Frequency histogram showing velocities of anterograde and retrograde axonal vesicles in vehicle- (grey bars) and latrunculin- (white bars) treated neurons. I, Nocodazole treatment results in a significant decrease in average velocity of all moving vesicles in axons. J, Nocodazole treatment significantly decreases the percentage of moving vesicles. K, Nocodazole treatment significantly increases the pausing time of moving vesicles. Latrunculin A treatment has no significant effect on average velocity, percentage mobile vesicles and pausing time of GFP–Sema3A vesicles. Values obtained for vehicle-treated neurons do not differ significantly from untreated neurons (data not shown). Bar graphs show mean ± SEM. $N = 9$ neurons, 224 vesicles tracked (dmso); $n = 10$ neurons, 267 vesicles tracked (noco); and $n = 9$ neurons, 230 vesicles tracked (lat. A). Statistical significance was determined using Student's *t*-test, and overall group differences were analyzed using one-way analysis of variance (ANOVA). *$p < 0.05$; **$p < 0.01$. Scale bar in (A–F) is 20 μm.

been shown to disrupt neuronal morphology to such an extent that the actin cytoskeleton appears to be affected as well (29). Treatment with the actin filament depolymerizing drug latrunculin A (5 μM) strongly reduced actin-labeling (Figure 6F) but left the microtubule network intact (Figure 6C).

Following nocodazole treatment, anterograde and retrograde GFP–Sema3A transport in axons was strongly reduced (Table 2). The frequency histogram in Figure 6G shows a significant shift toward lower velocities for both retrograde and anterograde moving vesicles in nocodazole-treated neurons compared with vehicle-treated cells (Figure 6G; $p < 0.05$, KS test). Nocodazole treatment significantly reduced the average velocity of all GFP–Sema3A axonal vesicles (0.71 ± 0.07 μm/s in vehicle-treated cells versus 0.45 ± 0.07 μm/s in nocodazole-treated cells; $p = 0.024$; Figure 6I). In addition, the percentage of moving vesicles was reduced in nocodazole-treated cells ($67.5 \pm 5.1\%$ in vehicle-treated cells versus $30.0 \pm 7.2\%$ in nocodazole-treated cells; $p = 0.001$; Figure 6J). Furthermore, nocodazole treatment resulted in an increase in pausing time ($14.0 \pm 3.3\%$ in vehicle-treated cells versus $24.9 \pm 4.7\%$ in nocodazole-treated cells; $p = 0.018$; Figure 6K). In contrast, none of these parameters was affected by treatment with latrunculin A. The velocities of anterograde and retrograde vesicles in latrunculin A-treated cells showed a similar distribution as in vehicle-treated cells (Figure 6H; $p > 0.05$, KS test). Average velocity, percentage moving vesicles and pausing time were not significantly different in latrunculin A-treated cells (Figure 6I–K and Table 2). Thus, disruption of the microtubule network, but not of actin filaments, reduced the average velocity and mobility and increased the pausing time of GFP–Sema3A vesicles.

GFP–Sema3A trafficking is activity dependent

We next examined whether trafficking of GFP–Sema3A in cortical neurons depends on neuronal activity. Neurons were transferred to the imaging chamber and subsequently imaged in depolarizing Tyrode's solution containing 60 mM KCl. Depolarization strongly reduced the average velocity of GFP–Sema3A vesicles in axons (0.70 ± 0.05 μm/s in control neurons versus 0.33 ± 0.04 μm/s in depolarized neurons; $p < 0.001$; Figure 7A and Table 3). The effect of 60 mM KCl-induced depolarization on the velocity of moving vesicles was dependent on the presence of Ca^{2+} in the extracellular medium, because imaging in Tyrode's containing 60 mM KCl, 5 mM EGTA and 0 mM Ca^{2+} did not significantly affect the velocity of moving vesicles in axons (Figure 7A). Conversely, blocking action potentials with 1 μM tetrodotoxin (TTX) caused an increase in the average velocity of axonal moving vesicles (0.70 ± 0.05 μm/s in control neurons versus 1.13 ± 0.10 μm/s in TTX-treated neurons; $p = 0.0028$; Figure 7A). Similar effects were found when the percentage mobile vesicles was analyzed in axons of depolarized and TTX-treated neurons. Depolarization induced a strong decrease in the percentage moving vesicles in axons ($65.5 \pm 4.2\%$ in control neurons versus $21.0 \pm 4.9\%$ in depolarized cells; $p < 0.001$; Figure 7B). Treatment with TTX caused a significant increase in the percentage of mobile vesicles ($65.5 \pm 4.2\%$ in control neurons versus $78.8 \pm 3.7\%$ in TTX-treated cells; $p = 0.0296$; Figure 7B). Analysis of the velocity profile of anterograde and retrograde moving vesicles in axons showed a significant shift toward lower velocities in 60 mM KCl-treated cells (Figure 7C; $p < 0.001$, KS test) and a significant shift toward higher velocities in TTX-treated cells (Figure 7D; $p < 0.001$, KS test). Both retrograde and anterograde moving vesicles were affected by these treatments (Figure 7C,D and Table 3). The velocity profile of axons imaged in 5 mM EGTA and 0 mM Ca^{2+} did not differ significantly from controls ($p > 0.05$, KS test).

In contrast to the activity-dependent trafficking of GFP–Sema3A vesicles in axons, dendritic GFP–Sema3A trafficking was largely unaffected by neuronal activity. Depolarizing neurons with 60 mM KCl or blockade of action potentials with TTX had no significant effect on the velocity of GFP–Sema3A vesicles in dendrites (Figure 7E and Table 4). In dendrites, depolarization caused a significant decrease in the percentage of moving vesicles ($41.8 \pm 3.7\%$ in control neurons versus $25.6 \pm 3.7\%$ in depolarized neurons; $p = 0.0072$; Figure 7F). Treatment with TTX did not affect the percentage moving vesicles in dendrites (Figure 7F). The distribution of velocities of anterograde and retrograde vesicles did not differ significantly in 60 mM KCl-, TTX- or 5 mM EGTA, 0 mM Ca^{2+}-treated dendrites (data not shown). Thus, neuronal activity strongly affects both velocity and mobility of GFP–Sema3A vesicles in axons but has a relatively minor effect on GFP–Sema3A trafficking in dendrites. Increased neuronal activity results in reduced axonal transport of GFP–Sema3A, whereas reduced neuronal activity causes an increase in GFP–Sema3A transport in axons.

Depolarization significantly reduced the percentage mobile vesicles in both axons and dendrites (Figure 7B,F and Tables 3 and 4). To test whether the increased number of stationary vesicles in stimulated neurons correlates with an increased Sema3A secretion, we took advantage of GFP–Sema3A's cell surface binding properties (Figure 4). GFP–Sema3A-transfected neurons were stimulated for 5 min with control or 60 mM KCl-containing Tyrode's in the presence of anti-GFP Ab. Depolarization resulted in an increase in the number of GFP–Sema3A surface puncta along neuronal processes (Figure 7G). Quantification of the number of surface puncta per length of MAP2-positive neurite showed a significant increase in Sema3A surface expression in depolarized neurons (4.9 ± 1.2 surface puncta in control neurons versus 10.9 ± 2.2 surface puncta per 100 μm MAP2-positive neurite in depolarized neurons; $p = 0.0291$; Figure 7H). Thus, the increased number of stationary vesicles in

Table 2: Axonal transport of GFP–Sema3A following disruption of the cytoskeleton

	Vehicle		Nocodazole		Latrunculin A	
	Velocity (μm/s)	% of total	Velocity (μm/s)	% of total	Velocity (μm/s)	% of total
Anterograde	0.73 ± 0.04	51.3	0.49 ± 0.03	26.2	0.79 ± 0.04	42.6
Retrograde	0.58 ± 0.06	12.1	0.62 ± 0.14	2.3	0.66 ± 0.05	17.4
Bi-directional	0.43 ± 0.06	4.0	0.46 ± 0.15	1.1	0.62 ± 0.11	3.0
Stationary	–	32.6	–	70.4	–	37.0

Vehicle: $n = 9$ neurons, 224 vesicles tracked; nocodazole (10 μM): $n = 10$ neurons, 267 vesicles tracked; latrunculin A (5 μM): $n = 9$ neurons, 230 vesicles tracked. Values represent mean ± SEM.

processes of depolarized cells correlates with an increased secretion of GFP–Sema3A.

Depolarization induces a reversible arrest of anterograde and retrograde axonal trafficking

To determine whether the depolarization-induced arrest in axonal trafficking of GFP–Sema3A was reversible, we applied a brief 30 s pulse of 60 mM KCl Tyrode's delivered from a pipette positioned near the imaged cell. Figure 8A shows frames of a time-lapse movie of GFP–Sema3A trafficking in an axonal segment (*Supplementary* Movie 3). Depolarization induced a rapid and robust decrease in axonal transport, which increased again after the stimulus had ended (Figure 8A, *Supplementary* Movie 3). Kymograph analysis showed that the trajectories of most moving vesicles were altered upon stimulus (Figure 8B). After the onset of depolarization, anterograde vesicles transiently slowed down (vesicle 2) or became stationary (vesicle 3). A similar decrease in velocity was observed for retrograde moving vesicles (vesicle 1). Vesicles accelerated again with various delays after the stimulus had ended, causing the reappearance of downward sloping lines corresponding to fast, anterograde moving vesicles in the kymograph (Figure 8B). The trajectories of vesicles in axons stimulated with a 30 s pulse of non-depolarizing control Tyrode's were unaltered (data not shown).

Comparison of the velocity profiles of vesicles before and during stimulus showed a significant shift toward lower values for both anterograde and retrograde traffic during depolarization (Figure 8C; $p < 0.001$, KS test). Vesicles showed a normal distribution of anterograde and retrograde velocities after the stimulus had ended (Figure 8D; $p > 0.05$, KS test). Quantification showed significant reductions in both the average velocity (0.80 ± 0.09 μm/s before versus 0.32 ± 0.03 μm/s during stimulus; $p < 0.001$; Figure 8E) and the percentage moving vesicles (82.4 ± 4.8% before versus 52.7 ± 5.6% during stimulus; $p < 0.01$; Figure 8F) during the 60 mM KCl stimulus. Average velocity and percentage moving vesicles returned to control values after the stimulus had ended (Figure 8E,F). Delivery of a train of action potentials (1800 AP, 30 Hz) induced a similar transient decrease in the average velocity of axonal vesicles (Figure 8G). The percentage moving vesicles in axons and the velocity and percentage moving vesicles in dendrites were not affected by field stimulation (data not shown). Thus, depolarization causes a reversible arrest of axonal trafficking of GFP–Sema3A.

Discussion

In this study, we investigated the localization and trafficking of the secreted semaphorin Sema3A in cortical neurons. Sema3A displayed a punctate distribution in axons and dendrites, which was closely reproduced by GFP–Sema3A. Live-cell imaging revealed distinct differences in the dynamics of GFP–Sema3A trafficking in axons and dendrites. Furthermore, axonal trafficking of GFP–Sema3A was strongly dependent on neuronal activity, whereas dendritic transport of GFP–Sema3A was not. Thus, both the dynamics and the activity dependence of GFP–Sema3A trafficking in cortical neurons differ between axons and dendrites, indicating that axons and dendrites regulate trafficking of Sema3A vesicles in distinct ways.

Differential dynamics of Sema3A vesicular trafficking in axons and dendrites

Expression of GFP–Sema3A or mRFP–Sema3A in neurons invariably resulted in a punctate distribution in axons and dendrites, which closely reproduced that of endogenous Sema3A. These puncta co-localized extensively with exogenously expressed secretory vesicle cargo proteins tPA–GFP or NPY–Venus. Both tPA–GFP and NPY–Venus are sorted into the regulated secretory pathway and are transported in large dense core vesicles (LDCVs) in cultured hippocampal neurons and neuroendocrine cells (24–27). Ultrastructural studies confirm that endogenous NPY localizes to LDCVs in rat brain as well (30,31). The observed co-localization with established secretory vesicle markers suggests that Sema3A can be sorted into the regulated pathway of secretion in neurons. In agreement with this, endogenous Sema3A displayed a partial co-localization with SgII, a marker for secretory vesicles (32). The remaining Sema3A puncta that did not co-localize with SgII might represent membrane-associated Sema3A, although we were unable to label endogenous surface Sema3A. Alternatively, these puncta could represent Sema3A in secretory vesicles that lack SgII. The granin composition of secretory vesicles can vary between individual cells (32,33), and SgII labels only a subpopulation of secretory

vesicles in non-neuronal cells (34). We were unable to distinguish between immature or mature secretory vesicles, because a SgII Ab that distinguishes between these types of secretory vesicles in PC12 cells (35) did not work on cortical neurons. Interestingly, the co-localization between Sema3A and secretory vesicle cargoes tPA and NPY suggests that proteins as diverse as NPY, a small peptide, and Sema3A, a large glycoprotein, may be stored in the same vesicle, co-transported to their destination and co-released upon the same stimulus.

Live-cell imaging revealed a highly dynamic behavior of secretory vesicles carrying GFP–Sema3A. The observed rapid movements, interrupted by stationary periods, and

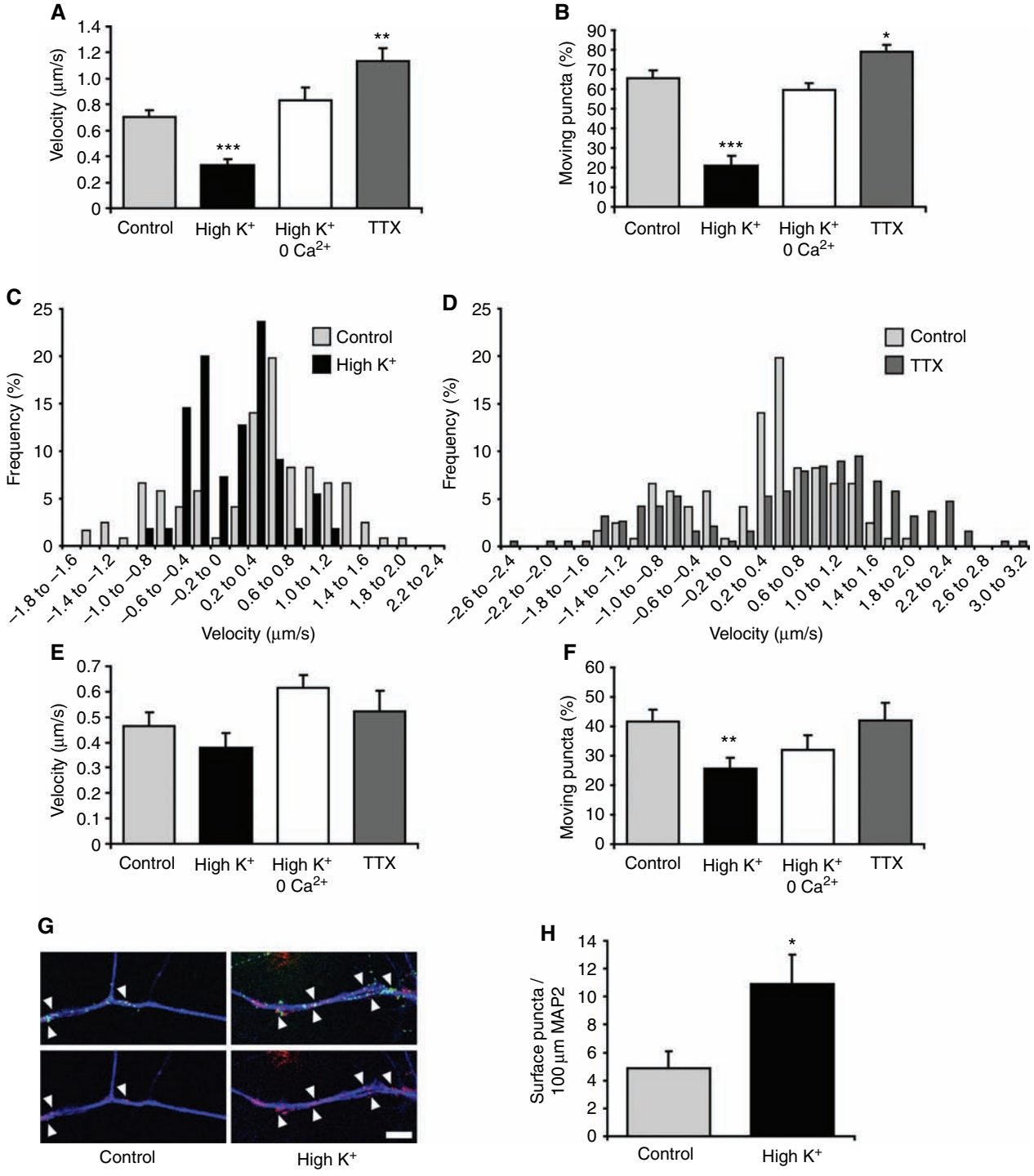

Figure 7: Legend continued on next page

Table 3: Axonal transport of GFP–Sema3A following depolarization or activity blockade

	Control		High K^+		High K^+ 0 Ca^{2+}		TTX	
	Velocity (μm/s)	% of total	Velocity (μm/s)	% of total	Velocity (μm/s)	% of total	Velocity (μm/s)	% of total
Anterograde	0.70 ± 0.04	41.6	0.39 ± 0.05	10.0	0.90 ± 0.07	32.0	1.24 ± 0.05	56.4
Retrograde	0.73 ± 0.07	16.3	0.39 ± 0.04	8.3	0.84 ± 0.06	24.5	1.01 ± 0.07	19.6
Bi-directional	0.54 ± 0.11	4.8	0.38 ± 0.08	2.7	0.72 ± 0.22	2.1	0.85 ± 0.23	2.8
Stationary	–	33.3	–	79.0	–	41.4	–	21.2

Control (Tyrode's): $n = 8$ neurons, 209 vesicles tracked; high K^+(60 mM KCl): $n = 12$ neurons, 300 vesicles tracked; high K^+ 0 Ca^{2+}(60 mM KCl, 0 mM Ca^{2+}, 5 mM EGTA): $n = 11$ neurons, 278 vesicles tracked; TTX (1 μM): $n = 10$ neurons, 250 vesicles tracked. Values represent mean ± SEM.

Table 4: Dendritic transport of GFP–Sema3A following depolarization or activity blockade

	Control		High K^+		High K^+ 0 Ca^{2+}		TTX	
	Velocity (μm/s)	% of total	Velocity (μm/s)	% of total	Velocity (μm/s)	% of total	Velocity (μm/s)	% of total
Anterograde	0.44 ± 0.06	12.0	0.41 ± 0.06	8.4	0.66 ± 0.09	12.0	0.49 ± 0.06	13.2
Retrograde	0.61 ± 0.07	17.3	0.41 ± 0.06	10.2	0.59 ± 0.08	12.0	0.57 ± 0.06	16.1
Bi-directional	0.33 ± 0.04	10.3	0.35 ± 0.04	6.6	0.64 ± 0.08	8.0	0.52 ± 0.08	12.6
Stationary	–	60.4	–	74.8	–	68.0	–	58.1

Control (Tyrode's): $n = 9$ neurons, 225 vesicles tracked; high K^+(60 mM KCl): $n = 11$ neurons, 274 vesicles tracked; high K^+ 0 Ca^{2+}(60 mM KCl, 0 mM Ca^{2+}, 5 mM EGTA): $n = 9$ neurons, 225 vesicles tracked; TTX (1 μM): $n = 7$ neurons, 174 vesicles tracked. Values represent mean ± SEM.

sudden reversals of direction are consistent with previous observations of microtubule-based transport in non-neuronal cells (36–39). Indeed, axonal transport of GFP–Sema3A was dependent on the integrity of the microtubule cytoskeleton. In contrast, disruption of actin filaments did not affect GFP–Sema3A axonal transport. However, our data do not exclude a role for actin-based local trafficking in the F-actin cortex near the cell membrane (40,41). The axonal and dendritic trafficking of secretory vesicles in neurons is poorly characterized, as most studies have relied on the use of neuroendocrine cells to study vesicle transport (24,41–43). We show here that distinct differences exist between secretory vesicle transport in the axonal and the dendritic domain with regard to directionality, velocity, mobility and pausing time. Axonal secretory vesicles undergo rapid anterograde transport toward distant terminals, whereas dendritic vesicles are largely stationary or move slowly, with no clear preference for the anterograde or retrograde direction. This divergence in axonal and dendritic vesicular trafficking may be due to several reasons. First, microtubules in axons are of uniform polarity, with their plus ends oriented away from the cell body, whereas dendrites contain microtubules of mixed polarity (44,45). The different microtubule organization in these two

Figure 7: Trafficking of GFP–Sema3A in cortical neurons is activity dependent. Neurons (DIV 14–15) were imaged in Tyrode's solution (control); in depolarizing Tyrode's-containing 60 mM KCl (high K^+); in Tyrode's-containing 60 mM KCl, 5 mM EGTA and 0 mM Ca^{2+} (high K^+ 0 Ca^{2+}) or in Tyrode's-containing 1 μM TTX. Application of 60 mM KCl Tyrode's effectively destained FM 4-64-loaded synapses (data not shown). Prolonged KCl-induced depolarization (1 h) in the presence or absence of Ca^{2+} did not affect the viability of neurons, based on propidium iodide staining (data not shown). A–D, Axonal trafficking; E,F, Dendritic trafficking. A, 60 mM KCl-induced depolarization results in a strong decrease in the average velocity of moving vesicles in axons compared with control neurons. Treatment with 1 μM TTX significantly increases the average velocity. B, Depolarization induces a significant decrease in the percentage moving vesicles in axons, whereas TTX has the opposite effect. C, Frequency histogram showing velocities of anterograde and retrograde (indicated as negative values) moving vesicles in axons of control (grey bars) and 60 mM KCl- (black bars) treated neurons. D, Frequency histogram showing velocities of anterograde and retrograde axonal vesicles in control (grey bars) and TTX- (dark grey bars) treated neurons. E, The average velocity of moving vesicles in dendrites is not affected by depolarization or TTX. F, Depolarization significantly decreases the percentage moving vesicles in dendrites. Data based on 8–12 neurons per condition for axonal transport, 1037 vesicles tracked; 7–11 neurons per condition for dendritic transport, 898 vesicles tracked. G,H, Depolarization increases GFP–Sema3A surface expression. G, Representative dendrites of control (left panel) and 60 mM KCl- (right panel) treated neurons (DIV 14), transfected with GFP–Sema3A (green), surface stained with anti-GFP (red) and labeled with anti-MAP2 (blue) following permeabilization. Dendrites are shown with (top) and without (bottom) GFP–Sema3A signal. Arrowheads indicate surface puncta. Scale bar, 5 μm. H, Depolarization results in a significant increase in the number of GFP–Sema3A surface puncta per 100 μm dendrite ($n = 8$ neurons per condition, 306 puncta). Bar graphs show mean ± SEM. Statistical significance was determined using Student's *t*-test, and overall group differences were analyzed using one-way analysis of variance (ANOVA). *$p < 0.05$; **$p < 0.01$; ***$p < 0.001$.

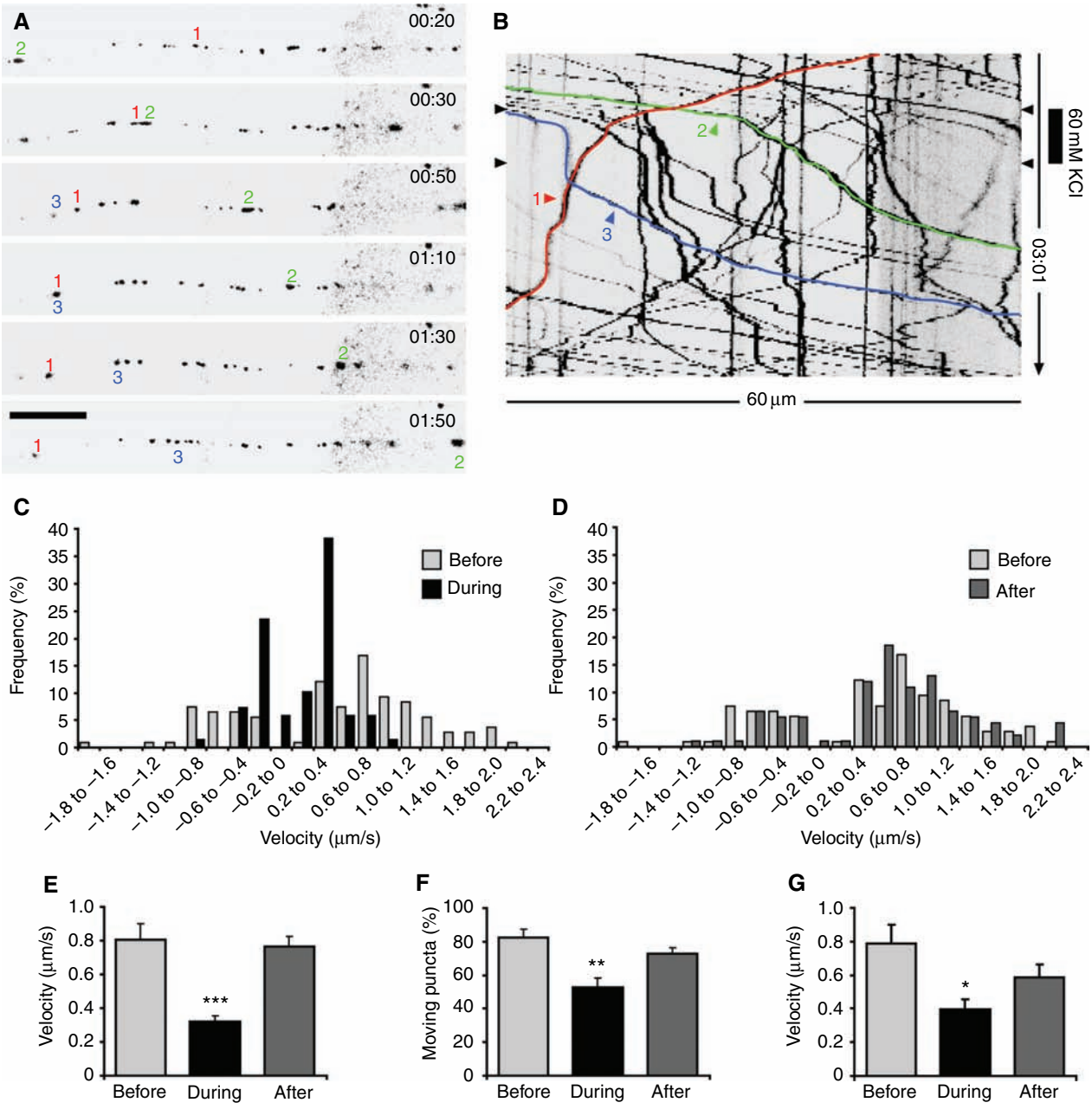

Figure 8: Depolarization induces a reversible arrest in axonal trafficking of GFP–Sema3A. A brief 30-s depolarizing pulse of 60 mM KCl Tyrode's was applied to the cells (DIV 14–15) after 30 s of imaging; neurons were imaged for an additional 2 min. A, Frames from time-lapse movie of axonal GFP–Sema3A trafficking. Cell body located to the left outside of the picture frame. Images have been inverted. Numbers indicate the positions of a retrograde vesicle (1, red) and two anterograde vesicles (2, green; 3, blue). B, Kymograph of the axonal segment shown in (A). The trajectories of the numbered vesicles indicated in (A) are highlighted in the corresponding colors. Anterograde vesicles appear as downward sloping lines. The onset and end of the stimulus are indicated by black arrowheads on either side of the kymograph and the black bar on the right. The trajectories of most moving vesicles are altered upon the onset of stimulus. C, Frequency histogram showing velocities of anterograde and retrograde (indicated as negative values) moving vesicles in the same axonal segment before (grey bars) and during (black bars) stimulus. 'Before' was defined as the last 10 frames before onset of stimulus; 'during' was defined as the last 10 frames of the 30-s stimulus. D, Frequency histogram showing velocities of anterograde and retrograde vesicles in the same axonal segment before (grey bars) and after (dark grey bars) stimulus. 'After' was defined as the last 10 frames of the time-lapse movie. E, The average velocity of GFP–Sema3A vesicles shows a significant decrease during stimulus. F, The percentage moving puncta is significantly decreased during stimulus. G, The average velocity of GFP–Sema3A vesicles shows a significant decrease during field stimulus (1800 action potentials, 30 Hz). The field stimulus used effectively destained FM 4-64-loaded presynaptic terminals (data not shown). Bar graphs show mean ± SEM. $N = 6$ neurons for 60 mM KCl-stimulated cells, 404 vesicles tracked; $n = 5$ neurons for field-stimulated cells, 374 vesicles tracked. Statistical significance was determined using Student's *t*-test, and overall group differences were analyzed using one-way analysis of variance (ANOVA). *$p < 0.05$; **$p < 0.01$; ***$p < 0.001$. Scale bar in (A) is 10 µm.

domains may account for the net anterograde trafficking of axonal vesicles and the lack of significant net anterograde or retrograde transport of vesicles in proximal dendrites. The high proportion of bi-directionally moving vesicles in dendrites may also result from the mixed polarity of microtubules in dendrites causing vesicles to change track more frequently than in axons, which could also account for the longer pausing time between dendritic vesicle movements. Second, a differential distribution of MAPs, which can interfere with vesicle movement along microtubules (46–49), could contribute to different dynamics of secretory vesicle trafficking in axons and dendrites. Third, a polarized distribution of motor proteins might contribute to the difference in vesicle trafficking in axons and dendrites (50). The frequency histogram in Figure 5 shows a distinct population of fast anterogradely moving vesicles in axons. The average velocity in the anterograde direction in axons is in agreement with fast axonal transport (51), which is carried out by kinesin family member (KIF) proteins (52,53). In *Caenorhabditis elegans*, the fast anterograde axonal transport of LDCVs was shown to depend in part on the microtubule motor UNC-104 (KIF1A) (54). It is not known which kinesins mediate secretory granule trafficking in vertebrate neurons (50).

Activity-dependent trafficking of Sema3A in axons

Previous studies investigating the effects of secretagogues on vesicle motility in neuroendocrine cells have produced conflicting results. Elevation of intracellular Ca^{2+} or Ba^{2+} levels increases secretory granule movement in PC12 cells (43,55) but has no effect on secretory granule trafficking in NS20Y cells (42). Results on secretory granule transport and exocytosis obtained in cell lines may not always translate to neurons (25). We find that in cortical neurons, depolarization caused a strong, reversible decrease of GFP–Sema3A trafficking in axons. Conversely, blockade of action potentials resulted in an increase in axonal GFP–Sema3A transport. Interestingly, depolarization altered the velocity and mobility of anterograde, as well as retrograde moving vesicles in axons. The finding that both anterograde and retrograde trafficking are affected suggests that the function of kinesin (mediating plus-end–oriented transport along microtubules) and dynein (mediating minus-end–oriented transport along microtubules) motor proteins was altered upon depolarization. The cellular mechanisms that regulate motor function are still incompletely understood, but phosphorylation appears to be one important mechanism to control kinesin and dynein motor proteins (56,57). Phosphorylation of kinesin light chains, through a signaling cascade involving cyclin-dependent kinase 5 (cdk5) and glycogen synthase kinase 3 (GSK3), inhibits kinesin-based motility and leads to the dissociation of kinesin from transport vesicles (58,59). Thus, kinesin function can be regulated by cell-signaling pathways. Other regulators of kinesin-based motility are cAMP (60) and calmodulin (61). Calcium-dependent binding of calmodulin negatively regulates kinesin-based motility, either by decreasing its motor function (61) or by inhibiting its binding to microtubules (62,63). This mechanism could provide a link between depolarization-induced Ca^{2+} influx and reduction of anterograde axonal trafficking mediated by kinesins. Dyneins are complex proteins consisting of multiple subunits, and the regulation of dynein motility can occur at multiple levels (57). Mechanisms regulating dynein-based retrograde trafficking include phosphorylation (64–66) and interacting proteins such as dynactin (67,68). Alternatively, neuronal activity could modify substrate properties such as the phosphorylation state of MAPs, thereby altering the regulation of vesicle trafficking along microtubules by MAPs. Inhibition of GSK3-mediated phosphorylation of tau, the major MAP in axons, results in an inhibition of anterograde organelle transport in PC12 cells (69).

Regulation of secretory vesicle trafficking by neuronal activity could serve to control the delivery of vesicle cargo to specific locations. The reversible arrest of trafficking during depolarization could indicate a transient fusion of vesicles with the plasma membrane. In line with this, we found that the increased number of stationary vesicles in processes of depolarized neurons correlated with an increased number of Sema3A surface puncta. This suggests that during stimulus, axonal vesicles might slow down and release their cargo along the axon, re-endocytose again (26,27) and move on when the stimulus has ended. Thus, a localized stimulus could induce a local release from Sema3A carrying vesicles. A similar cycling with the plasma membrane during transport has been suggested for vesicles transporting N-methyl-D-aspartate receptor subunits in young neurons (70). Apparently, the mechanisms that regulate axonal secretory vesicle trafficking do not operate to the same extent in dendrites. The dendritic transport of GFP–Sema3A may be carried out by motor proteins that lack regulation by signaling pathways or neuronal activity.

The difference in both the dynamics and the activity dependence of GFP–Sema3A trafficking in axons and dendrites raises the question whether these characteristics also affect release of Sema3A from these two compartments. Surface-bound GFP–Sema3A puncta were found both on axons and on dendrites, suggesting that Sema3A can be secreted from both compartments. Work in neuroendocrine cells has shown that LDCV secretion is limited by vesicle mobility (55,71,72). In hippocampal neurons, secretory vesicles near the plasma membrane display substantial movement before fusion (25). The rapid activity-dependent anterograde transport of secretory vesicles in axons suggests that the axonal compartment is the predominant site for Sema3A secretion, in contrast to dendrites where vesicles move slowly or remain stationary. Future work should determine whether the dynamics of Sema3A release differ between the axonal and the dendritic domain and whether the activity-dependent release of secreted semaphorins can occur at synaptic sites.

Materials and Methods

Plasmids and reagents

The GFP–Sema3A expression plasmid has been described previously and has been shown to retain its biological activity (22). A red fluorescent version of Sema3A was generated by replacing enhanced green fluorescent protein with mRFP (73). Primers were designed to place a *Nhe*I restriction site at the 5′ end of mRFP and a *Bam*HI site at the 3′ end. Primers were mRFP 5′-GCCGCTAGCGCCTCCTCCGAGGACGTCATCAA and mRFP 3′-GCCGGATCCGGCGCCGGTGGAGTGGCG. The mRFP fragment resulting from PCR amplification was digested with *Nhe*I and *Bam*HI and cloned into the GFP–Sema3A expression plasmid from which EGFP had been excised. NPY–Venus expression plasmid was kindly provided by Dr A. Miyawaki (Brain Science Institute, RIKEN, Japan). The tPA–GFP expression plasmid was generously provided by Dr B. A. Scalettar (Lewis and Clark College, Portland, OR, USA). Nocodazole was from Sigma (Zwijndrecht, the Netherlands). TTX was from Alomone labs (Jerusalem, Israel). Alexa Fluor 647-conjugated transferrin and latrunculin A were from Molecular Probes (Leiden, the Netherlands).

Cell culture and transfections

Cerebral cortices from C57/Bl6 mouse E18 embryos were dissected free of meninges in Hanks' Balanced Salt Solution (HBSS; Gibco BRL, Breda, the Netherlands) containing 7 mM HEPES and digested with 0.25% trypsin (Gibco) in HBSS for 15 min at 37 °C. Tissue was washed three times in HBSS/HEPES and triturated with a fire-polished glass pipette. Dissociated neurons were plated at a density of 50.000 cells/well on top of a layer of rat glial cells grown at a density of 25.000 cells/well on 18 mm glass coverslips (Menzel Glaser, Braunschweig, Germany) in 12-well plates. Cells were grown in Neurobasal medium (Gibco) supplemented with B27 (Gibco), 18 mM HEPES, 0.5 mM Glutamax (Gibco), 25 μM ß-mercaptoethanol and penicillin/streptomycin (Gibco). Half of the medium was replaced once a week. Calcium phosphate transfections were done as described (74). Cells were routinely transfected at 6–8 DIV and imaged between 14 and 17 DIV.

Immunocytochemistry

Cells were fixed in 4% paraformaldehyde (Sigma) in PBS (pH 7.4) for 20 min at room temperature. Cells were washed in PBS and blocked in PBS–FBS [PBS containing 5% FBS (Gibco), 0.2% Triton X-100] for 1 h at room temperature. Incubations with primary Abs were done overnight at 4 °C in PBS–FBS. Primary Abs used were Sema3A C-17 polyclonal Ab (pAb) [Santa Cruz Biotechnology, Santa Cruz, CA, USA; Sema3A N-15 pAb and H-300 pAb from Santa Cruz Biotechnology yielded a similar punctate distribution in cortical neurons (not shown)], MAP2 monoclonal Ab (mAb) and pAb (Chemicon, Harrow, UK), SgII pAb (32) (generously provided by Dr P. Rosa, Institute of Neuroscience, Center of Cellular and Molecular Pharmacology, Milan, Italy), alpha-tubulin mAb (Synaptic Systems, Goettingen, Germany) and synapsin I and II pAb (E028). Rhodamine–phalloidin (Molecular Probes) was used to visualize actin. Alexa Fluor-conjugated secondary Abs were from Molecular Probes. After several washes, coverslips were mounted in ProLong antifade reagent (Molecular Probes) and examined on a Zeiss LSM 510 confocal laser scanning microscope. Specificity of staining was confirmed by omission of the primary Ab. For live-cell labeling, GFP–Sema3A-transfected neurons were briefly washed with PBS (37 °C) and incubated with GFP mAb (Chemicon) in PBS for 5 min at 37 °C. Subsequently, cells were washed two times in PBS and fixed in 4% paraformaldehyde in PBS for 20 min at room temperature. After three washes in PBS, cells were incubated with biotinylated anti-mouse Ab (mouse on mouse kit, Vector Laboratories, Burlingame, CA, USA) followed by an incubation with streptavidin-Alexa 546 (Molecular Probes) and mounting in ProLong antifade reagent.

Live-cell imaging and image analysis

Coverslips were placed in a chamber containing Tyrode's solution (2 mM $CaCl_2$, 2.5 mM KCl, 119 mM NaCl, 2 mM $MgCl_2$, 30 mM glucose, 25 mM HEPES, pH 7.4) and imaged on an Axiovert II microscope (Zeiss, Oberkochen, Germany) equipped with a heated stage (32 °C), a Coolsnap HQ camera (Photometrics, Tucson, AZ, USA) and a Polychrome IV illumination unit (TILL Photonics, Grafelfing, Germany). Images were acquired in MetaMorph 6.2 software (Universal Imaging, Downingtown, PA, USA) using a ×40 objective. Cells were depolarized with Tyrode's solution containing 60 mM KCl (2 mM $CaCl_2$, 60 mM KCl, 61.5 mM NaCl, 2 mM $MgCl_2$, 30 mM glucose, 25 mM HEPES, pH 7.4). Tyrode's containing 0 mM Ca^{2+} and 5 mM EGTA was used as a control (0 mM $CaCl_2$, 5 mM EGTA, 60 mM KCl, 61.5 mM NaCl, 4 mM $MgCl_2$, 30 mM glucose, 25 mM HEPES, pH 7.4). Field stimulation was applied through parallel platinum electrodes immersed into the perfusion chamber, delivering 30 mA, 1 ms pulses, using a Master8 stimulator (AMPI, Jerusalem, Israel) and a Stimulus Isolator A385 (World Precision Instruments, Sarasota, FL, USA).

Axons and dendrites were distinguished based on their distinct morphological characteristics (75). Only dendrites that could be identified by their typical thick, tapering diameter and retraced to the cell body of transfected cells were included in the analysis; dendrites with a fasciculating axon that also contained fluorescent puncta were excluded. Axons were identified by their uniform thin diameter and length, which considerably exceeded that of dendrites. Only single axons that were isolated from other fluorescently labeled processes and could be retraced to the cell body of transfected cells were included in the analysis. The identity of dendrites and axons identified in this way was confirmed by retrospective immunocytochemistry for the dendritic marker MAP2 for the cells analyzed to obtain a basal description of Sema3A trafficking.

Stacks from 1-min time-lapse recordings acquired with an interval of 1 s were used to analyze the dynamics of vesicle trafficking. Vesicle trafficking in dendrites was analyzed in proximal dendrites 20–100 μm away from the cell body; trafficking in axons was measured 20–200 μm away from the soma. The trajectories of moving puncta were determined by manual tracking using the 'track points' function in MetaMorph. Discrete puncta were tracked until they disappeared from view or could no longer be distinguished from other moving puncta (Figure 5). A vesicle was considered moving when it displayed movement for at least three consecutive frames; all other vesicles were qualified as stationary. The speed of moving vesicles was corrected for stationary periods and determined by dividing the total distance traveled by the time spent traveling. The 'distance to origin' function in MetaMorph was used to determine the direction of the trajectories. A vesicle had to display directed movement for at least two consecutive frames to be qualified as anterograde or retrograde. Vesicles that changed direction during the period that they could be tracked were qualified as bi-directional. In the experiments in which the cytoskeleton or cellular activity levels were manipulated (Figures 6–8), vesicle trafficking was quantified using the same criteria as described above but analyzing only the first 10 frames of the time-lapse sequence. The values obtained using this method were not significantly different from the values obtained from the analysis of entire sequences (data not shown). Each of the experiments described in Figures 5–7 contains its own group of control neurons, among which minor, non-significant variations can occur.

To determine co-localization of fluorescent puncta, single channels of red–green–blue confocal images were saved as separate monochrome TIFF images and thresholded in MetaMorph. Circular regions of 10 × 10 pixels were placed around individual puncta in one image, and these regions were transferred to the other image. Subsequently, co-localizing puncta were counted.

Quantification of Sema3A surface expression

Neurons were stimulated for 5 min at 37 °C with control Tyrode's or Tyrode's containing 60 mM KCl, in the presence of anti-GFP mAb. Following stimulation, cells were washed, fixed and incubated with biotinylated anti-mouse and streptavidin-Alexa 546 Abs. Subsequently, cells were permeabilized with Triton X-100 and labeled with anti-MAP2 pAb and Cy5-conjugated anti-rabbit Ab. Confocal images were taken with identical detector gain, amplifier offset and pinhole settings for all cells. The red channel image containing GFP–Sema3A surface staining was saved as a

separate TIFF file and imported into MetaMorph. Images were thresholded using identical threshold settings for all cells. Threshold was chosen, such that all recognizable surface puncta were included. All spots larger than 2 pixels were counted, and the length of neurites containing surface puncta was measured.

Acknowledgments

We thank Dr Bethe Scalettar for kindly providing the tPA–GFP plasmid and Dr Patrizia Rosa for generously providing the secretogranin II antibody. We thank Dr Martijn Roelandse for expert advice on image analysis and Desiree Schut for providing glial cell cultures.

Supplementary Material

Movie 1. GFP–Sema3A trafficking in an axon of a cortical neuron (17 DIV). Movie shows a 1-min time-lapse sequence, with images taken every second. Movie frames have been inverted for clarity. Cell body located to the left outside of the picture frame. Scale bar, 5 μm.

Movie 2. GFP–Sema3A trafficking in a dendrite of a cortical neuron (14 DIV). Movie shows a 1-min time-lapse sequence, with images taken every second. Movie frames have been inverted. Cell body located to the left outside of the picture frame. Scale bar, 5 μm.

Movie 3. GFP–Sema3A trafficking in an axon (DIV 15) before, during and after the application of a 30-s depolarizing (60 mM KCl) stimulus. Movie shows a 3-min time-lapse sequence, with images taken every second. Cells were imaged for 30 s, followed by a 30-s depolarizing stimulus. Cells were imaged for an additional 2 min after the stimulus had ended. Duration of stimulus is indicated in the movie. Movie frames have been inverted. Cell body located to the left outside of the picture frame. Scale bar, 10 μm.

These materials are available as part of the online article from http://www.blackwell-synergy.com

References

1. Fiore R, Puschel AW. The function of semaphorins during nervous system development. Front Biosci 2003;8:s484–s499.
2. Luo Y, Raible D, Raper JA. Collapsin: a protein in brain that induces the collapse and paralysis of neuronal growth cones. Cell 1993;75: 217–227.
3. Raper JA. Semaphorins and their receptors in vertebrates and invertebrates. Curr Opin Neurobiol 2000;10:88–94.
4. Pasterkamp RJ, Kolodkin AL. Semaphorin junction: making tracks toward neural connectivity. Curr Opin Neurobiol 2003;13:79–89.
5. Behar O, Golden JA, Mashimo H, Schoen FJ, Fishman MC. Semaphorin III is needed for normal patterning and growth of nerves, bones and heart. Nature 1996;383:525–528.
6. Taniguchi M, Yuasa S, Fujisawa H, Naruse I, Saga S, Mishina M, Yagi T. Disruption of semaphorin III/D gene causes severe abnormality in peripheral nerve projection. Neuron 1997;19:519–530.
7. Sahay A, Molliver ME, Ginty DD, Kolodkin AL. Semaphorin 3F is critical for development of limbic system circuitry and is required in neurons for selective CNS axon guidance events. J Neurosci 2003;23: 6671–6680.
8. Giger RJ, Cloutier JF, Sahay A, Prinjha RK, Levengood DV, Moore SE, Pickering S, Simmons D, Rastan S, Walsh FS, Kolodkin AL, Ginty DD, Geppert M. Neuropilin-2 is required in vivo for selective axon guidance responses to secreted semaphorins. Neuron 2000;25:29–41.
9. Chen H, Bagri A, Zupicich JA, Zou Y, Stoeckli E, Pleasure SJ, Lowenstein DH, Skarnes WC, Chedotal A, Tessier-Lavigne M. Neuropilin-2 regulates the development of selective cranial and sensory nerves and hippocampal mossy fiber projections. Neuron 2000;25:43–56.
10. Kitsukawa T, Shimizu M, Sanbo M, Hirata T, Taniguchi M, Bekku Y, Yagi T, Fujisawa H. Neuropilin-semaphorin III/D-mediated chemorepulsive signals play a crucial role in peripheral nerve projection in mice. Neuron 1997;19:995–1005.
11. Bagri A, Cheng HJ, Yaron A, Pleasure SJ, Tessier-Lavigne M. Stereotyped pruning of long hippocampal axon branches triggered by retraction inducers of the semaphorin family. Cell 2003;113:285–299.
12. de Wit J, Verhaagen J. Role of semaphorins in the adult nervous system. Prog Neurobiol 2003;71:249–267.
13. Fenstermaker V, Chen Y, Ghosh A, Yuste R. Regulation of dendritic length and branching by semaphorin 3A. J Neurobiol 2004;58:403–412.
14. Gu C, Rodriguez ER, Reimert DV, Shu T, Fritzsch B, Richards LJ, Kolodkin AL, Ginty DD. Neuropilin-1 conveys semaphorin and VEGF signaling during neural and cardiovascular development. Dev Cell 2003;5:45–57.
15. Giger RJ, Pasterkamp RJ, Heijnen S, Holtmaat AJ, Verhaagen J. Anatomical distribution of the chemorepellent semaphorin III/collapsin-1 in the adult rat and human brain: predominant expression in structures of the olfactory-hippocampal pathway and the motor system. J Neurosci Res 1998;52:27–42.
16. Holtmaat AJ, De Winter F, De Wit J, Gorter JA, da Silva FH, Verhaagen J. Semaphorins: contributors to structural stability of hippocampal networks? Prog Brain Res 2002;138:17–38.
17. Holtmaat AJ, Gorter JA, De Wit J, Tolner EA, Spijker S, Giger RJ, Lopes da Silva FH, Verhaagen J. Transient downregulation of Sema3A mRNA in a rat model for temporal lobe epilepsy. A novel molecular event potentially contributing to mossy fiber sprouting. Exp Neurol 2003;182:142–150.
18. Barnes G, Puranam RS, Luo Y, McNamara JO. Temporal specific patterns of semaphorin gene expression in rat brain after kainic acid-induced status epilepticus. Hippocampus 2003;13:1–20.
19. Sahay A, Kim CH, Sepkuty JP, Cho E, Huganir RL, Ginty DD, Kolodkin AL. Secreted semaphorins modulate synaptic transmission in the adult hippocampus. J Neurosci 2005;25:3613–3620.
20. Giger RJ, Wolfer DP, De Wit GM, Verhaagen J. Anatomy of rat semaphorin III/collapsin-1 mRNA expression and relationship to developing nerve tracts during neuroembryogenesis. J Comp Neurol 1996; 375:378–392.
21. Skaliora I, Singer W, Betz H, Puschel AW. Differential patterns of semaphorin expression in the developing rat brain. Eur J Neurosci 1998;10:1215–1229.
22. De Wit J, De Winter F, Klooster J, Verhaagen J. Semaphorin 3A displays a punctate distribution on the surface of neuronal cells and interacts with proteoglycans in the extracellular matrix. Mol Cell Neurosci 2005;29:40–55.
23. Fletcher TL, Cameron P, De Camilli P, Banker G. The distribution of synapsin I and synaptophysin in hippocampal neurons developing in culture. J Neurosci 1991;11:1617–1626.
24. Lochner JE, Kingma M, Kuhn S, Meliza CD, Cutler B, Scalettar BA. Real-time imaging of the axonal transport of granules containing a tissue plasminogen activator/green fluorescent protein hybrid. Mol Biol Cell 1998;9:2463–2476.
25. Silverman MA, Johnson S, Gurkins D, Farmer M, Lochner JE, Rosa P, Scalettar BA. Mechanisms of transport and exocytosis of dense-core granules containing tissue plasminogen activator in developing hippocampal neurons. J Neurosci 2005;25:3095–3106.
26. Taraska JW, Perrais D, Ohara-Imaizumi M, Nagamatsu S, Almers W. Secretory granules are recaptured largely intact after stimulated

exocytosis in cultured endocrine cells. Proc Natl Acad Sci USA 2003;100:2070–2075.
27. Tsuboi T, Rutter GA. Multiple forms of "kiss-and-run" exocytosis revealed by evanescent wave microscopy. Curr Biol 2003;13:563–567.
28. Nakata T, Terada S, Hirokawa N. Visualization of the dynamics of synaptic vesicle and plasma membrane proteins in living axons. J Cell Biol 1998;140:659–674.
29. Ligon LA, Steward O. Role of microtubules and actin filaments in the movement of mitochondria in the axons and dendrites of cultured hippocampal neurons. J Comp Neurol 2000;427:351–361.
30. Pelletier G, Guy J, Allen YS, Polak JM. Electron microscope immunocytochemical localization of neuropeptide Y (NPY) in the rat brain. Neuropeptides 1984;4:319–324.
31. Pickel VM, Chan J, Massari VJ. Neuropeptide Y-like immunoreactivity in neurons of the solitary tract nuclei: vesicular localization and synaptic input from GABAergic terminals. Brain Res 1989;476:265–278.
32. Rosa P, Hille A, Lee RW, Zanini A, De Camilli P, Huttner WB. Secretogranins I and II: two tyrosine-sulfated secretory proteins common to a variety of cells secreting peptides by the regulated pathway. J Cell Biol 1985;101:1999–2011.
33. Malosio ML, Giordano T, Laslop A, Meldolesi J. Dense-core granules: a specific hallmark of the neuronal/neurosecretory cell phenotype. J Cell Sci 2004;117:743–749.
34. Hashimoto S, Fumagalli G, Zanini A, Meldolesi J. Sorting of three secretory proteins to distinct secretory granules in acidophilic cells of cow anterior pituitary. J Cell Biol 1987;105:1579–1586.
35. Tooze SA, Hollinshead M, Dittie AS. Antibodies to secretogranin II reveal potential processing sites. Biochimie 1994;76:271–276.
36. Wacker I, Kaether C, Kromer A, Migala A, Almers W, Gerdes HH. Microtubule-dependent transport of secretory vesicles visualized in real time with a GFP-tagged secretory protein. J Cell Sci 1997;110:1453–1463.
37. Hirschberg K, Miller CM, Ellenberg J, Presley JF, Siggia ED, Phair RD, Lippincott-Schwartz J. Kinetic analysis of secretory protein traffic and characterization of golgi to plasma membrane transport intermediates in living cells. J Cell Biol 1998;143:1485–1503.
38. Toomre D, Keller P, White J, Olivo JC, Simons K. Dual-color visualization of trans-Golgi network to plasma membrane traffic along microtubules in living cells. J Cell Sci 1999;112:21–33.
39. Kreis TE, Matteoni R, Hollinshead M, Tooze J. Secretory granules and endosomes show saltatory movement biased to the anterograde and retrograde directions, respectively, along microtubules in AtT20 cells. Eur J Cell Biol 1989;49:128–139.
40. Bridgman PC. Myosin-dependent transport in neurons. J Neurobiol 2004;58:164–174.
41. Rudolf R, Salm T, Rustom A, Gerdes HH. Dynamics of immature secretory granules: role of cytoskeletal elements during transport, cortical restriction, and F-actin-dependent tethering. Mol Biol Cell 2001;12:1353–1365.
42. Washburn CL, Bean JE, Silverman MA, Pellegrino MJ, Yates PA, Allen RG. Regulation of peptidergic vesicle mobility by secretagogues. Traffic 2002;3:801–809.
43. Pouli AE, Emmanouilidou E, Zhao C, Wasmeier C, Hutton JC, Rutter GA. Secretory-granule dynamics visualized in vivo with a phogrin-green fluorescent protein chimaera. Biochem J 1998;333:193–199.
44. Baas PW, Deitch JS, Black MM, Banker GA. Polarity orientation of microtubules in hippocampal neurons: uniformity in the axon and nonuniformity in the dendrite. Proc Natl Acad Sci USA 1988;85: 8335–8339.
45. Baas PW, Black MM, Banker GA. Changes in microtubule polarity orientation during the development of hippocampal neurons in culture. J Cell Biol 1989;109:3085–3094.
46. Sheetz MP, Pfister KK, Bulinski JC, Cotman CW. Mechanisms of trafficking in axons and dendrites: implications for development and neurodegeneration. Prog Neurobiol 1998;55:577–594.
47. Sanchez C, Diaz-Nido J, Avila J. Phosphorylation of microtubule-associated protein 2 (MAP2) and its relevance for the regulation of the neuronal cytoskeleton function. Prog Neurobiol 2000;61:133–168.
48. Bulinski JC, McGraw TE, Gruber D, Nguyen HL, Sheetz MP. Overexpression of MAP4 inhibits organelle motility and trafficking in vivo. J Cell Sci 1997;110:3055–3064.
49. Sato-Harada R, Okabe S, Umeyama T, Kanai Y, Hirokawa N. Microtubule-associated proteins regulate microtubule function as the track for intracellular membrane organelle transports. Cell Struct Funct 1996;21:283–295.
50. Hirokawa N, Takemura R. Molecular motors and mechanisms of directional transport in neurons. Nat Rev Neurosci 2005;6:201–214.
51. Vallee RB, Bloom GS. Mechanisms of fast and slow axonal transport. Annu Rev Neurosci 1991;14:59–92.
52. Vale RD, Reese TS, Sheetz MP. Identification of a novel force-generating protein, kinesin, involved in microtubule-based motility. Cell 1985;42:39–50.
53. Brady ST. A novel brain ATPase with properties expected for the fast axonal transport motor. Nature 1985;317:73–75.
54. Zahn TR, Angleson JK, MacMorris MA, Domke E, Hutton JF, Schwartz C, Hutton JC. Dense core vesicle dynamics in Caenorhabditis elegans neurons and the role of kinesin UNC-104. Traffic 2004;5: 544–559.
55. Ng YK, Lu X, Levitan ES. Physical mobilization of secretory vesicles facilitates neuropeptide release by nerve growth factor-differentiated PC12 cells. J Physiol 2002;542:395–402.
56. Haimo LT. Regulation of kinesin-directed movements. Trends Cell Biol 1995;5:165–168.
57. Mallik R, Gross SP. Molecular motors: strategies to get along. Curr Biol 2004;14:R971–R982.
58. Morfini G, Szebenyi G, Elluru R, Ratner N, Brady ST. Glycogen synthase kinase 3 phosphorylates kinesin light chains and negatively regulates kinesin-based motility. Embo J 2002;21:281–293.
59. Morfini G, Szebenyi G, Brown H, Pant HC, Pigino G, DeBoer S, Beffert U, Brady ST. A novel CDK5-dependent pathway for regulating GSK3 activity and kinesin-driven motility in neurons. Embo J 2004;23: 2235–2245.
60. Sato-Yoshitake R, Yorifuji H, Inagaki M, Hirokawa N. The phosphorylation of kinesin regulates its binding to synaptic vesicles. J Biol Chem 1992;267:23930–23936.
61. Matthies HJ, Miller RJ, Palfrey HC. Calmodulin binding to and cAMP-dependent phosphorylation of kinesin light chains modulate kinesin ATPase activity. J Biol Chem 1993;268:11176–11187.
62. Vinogradova MV, Reddy VS, Reddy AS, Sablin EP, Fletterick RJ. Crystal structure of kinesin regulated by Ca(2+)-calmodulin. J Biol Chem 2004;279:23504–23509.
63. Reddy VS, Reddy AS. The calmodulin-binding domain from a plant kinesin functions as a modular domain in conferring Ca2+-calmodulin regulation to animal plus- and minus-end kinesins. J Biol Chem 2002;277:48058–48065.
64. Runnegar MT, Wei X, Hamm-Alvarez SF. Increased protein phosphorylation of cytoplasmic dynein results in impaired motor function. Biochem J 1999;342:1–6.
65. Dillman JF III, Pfister KK. Differential phosphorylation in vivo of cytoplasmic dynein associated with anterogradely moving organelles. J Cell Biol 1994;127:1671–1681.
66. Lin SX, Ferro KL, Collins CA. Cytoplasmic dynein undergoes intracellular redistribution concomitant with phosphorylation of the heavy chain in response to serum starvation and okadaic acid. J Cell Biol 1994;127:1009–1019.
67. Vaughan PS, Leszyk JD, Vaughan KT. Cytoplasmic dynein intermediate chain phosphorylation regulates binding to dynactin. J Biol Chem 2001;276:26171–26179.

68. Kumar S, Lee IH, Plamann M. Cytoplasmic dynein ATPase activity is regulated by dynactin-dependent phosphorylation. J Biol Chem 2000;275:31798–31804.
69. Tatebayashi Y, Haque N, Tung YC, Iqbal K, Grundke-Iqbal I. Role of tau phosphorylation by glycogen synthase kinase-3beta in the regulation of organelle transport. J Cell Sci 2004;117:1653–1663.
70. Washbourne P, Liu XB, Jones EG, McAllister AK. Cycling of NMDA receptors during trafficking in neurons before synapse formation. J Neurosci 2004;24:8253–8264.
71. Han W, Ng YK, Axelrod D, Levitan ES. Neuropeptide release by efficient recruitment of diffusing cytoplasmic secretory vesicles. Proc Natl Acad Sci USA 1999;96:14577–14582.
72. Burke NV, Han W, Li D, Takimoto K, Watkins SC, Levitan ES. Neuronal peptide release is limited by secretory granule mobility. Neuron 1997;19:1095–1102.
73. Campbell RE, Tour O, Palmer AE, Steinbach PA, Baird GS, Zacharias DA, Tsien RY. A monomeric red fluorescent protein. Proc Natl Acad Sci USA 2002;99:7877–7882.
74. Kohrmann M, Haubensak W, Hemraj I, Kaether C, Lessmann VJ, Kiebler MA. Fast, convenient, and effective method to transiently transfect primary hippocampal neurons. J Neurosci Res 1999; 58: 831–835.
75. Banker GA, Cowan WM. Further observations on hippocampal neurons in dispersed cell culture. J Comp Neurol 1979;187:469–493.